Journal of the European Ceramic Society **17** (1997) 33–39

PII: S0955-2219(96)00074-X
0955-2219/97/$17.00

Assessment of the Mechanical Behaviour of SiC Fibre Reinforced Magnesium Lithium Aluminosilicate Glass-Ceramic Matrix Composite Tested Under Uniaxial Tensile Loading

Monssef Drissi-Habti

LERMAT URA CNRS no 1317, ISMRA, 6 Bd du Maréchal Juin, 14050 Caen Cedex, France

(Received 20 January 1995; revised version received 28 March 1996; accepted 2 April 1996)

Abstract

The mechanical behaviour under quasi-static uniaxial tensile loading of SiC–MAS.L glass-ceramic composite material is investigated. The accumulation of damage in unidirectional specimens is characterized by the total number of transverse matrix cracks, N, *and the reduction in the longitudinal Young's modulus,* E. *The micromechanical parameters governing the matrix microcracking mechanism are calculated. © 1996 Elsevier Science Limited.*

1 Introduction

Ceramic matrix composites have received much attention during the last decade for structural applications mainly in aerospace and military components. In such materials, because the fibres have a larger strain to failure than the matrix, extensive matrix microcracking in the form of regularly spaced matrix cracks develops before ultimate failure. For material scientists, this damage capability is of prime interest for evaluating the mechanical behaviour of a material that is under development.

Since the well-known paper by Aveston, Cooper and Kelly (ACK) in 1971,[1] the description of the accumulation of damage in a composite material using the matrix microcracking mechanism has been subjected to many improvements.[2–4] This method, correlated to experimental observations, provides information on the ability of a composite under development to sustain damage and some ideas to improve its mechanical properties. In addition, since composites are candidates for high-temperature use, it is therefore of prime importance to detect the stress of first matrix cracking (and its corresponding strain).

The aim of this paper is to study the mechanical properties of SiC–MAS.L glass-ceramic composite, processed by Aérospatiale (Etablissement de Bordeaux), under uniaxial tensile loading. The first step involves a precise description of the damage sequence as a function of the applied load. The accumulation of damage is estimated using the number of transverse matrix microcracks (N). This damage parameter is then correlated to the stiffness reduction of the specimens. The last part of this work uses the transverse matrix microcracking results, in addition to the ACK model, to estimate the interfacial shear stress (τ), the matrix fracture energy release rate (Γ_m) and the critical flaw size (a^*) as defined by Marshall *et al.*[2]

2 Materials and Experiments

The materials were processed by Aérospatiale (Etablissement de Bordeaux, St Médard-en-Jalles, France), using a process route similar to that reported by Prewo.[5] They were made from continuous SiC fibres (NLM 202 Nicalon, Nippon Carbon, Japan) and a lithium magnesium aluminosilicate glass-ceramic matrix (MAS.L). The bundles of SiC fibres were infiltrated with a slurry of composition 0·5 MgO–0·5 Li_2O–1 Al_2O_3–4 SiO_2 by weight, obtained using a sol–gel route, to produce unidirectional plies in which the fibres were aligned parallel to one another. The pre-impregnated plies were then stacked and hot-pressed at a temperature of ~1300°C under an inert atmosphere. The hot-pressing temperature could be modulated to control the crystalline structure of the matrix.[6] The physical characteristics of the resulting composite material are listed in Table 1.

Table 1. Physical characteristics of the SiC–MAS.L composite material as given by Aérospatiale[6]

Composition of matrix	0·5 MgO–0·5 Li_2O–1 Al_2O_3–4 SiO_2
Type of fibre	SiC, Nicalon NLM 202
Fibre radius	R_f = 7·5 μm
Volume fraction of fibres	V_f = 0·33
Young's modulus of fibres	E_f = 200 GPa
Young's modulus of matrix	E_m = 70 GPa
Apparent density	ρ = 2500 kg m^{-3}
Number of plies	8
Longitudinal Young's modulus	123 GPa
Four-point bending strength	790 MPa
Tensile strength	400 MPa
Shear strength	16 MPa
Poisson's coefficient	ν = 0·23
Thermal expansion coefficient (20 to 1000°C)	
• parallel to fibres	3·4 × 10^{-6} °C^{-1}
• perpendicular to fibres	1·7 × 10^{-6} °C^{-1}

Dog-bone shaped specimens of total length l = 120 mm, with a gauge length L = 40 mm and a cross-section S = 16 mm^2, were machined from the plates. For each specimen, one large face and a side face were polished using different grades of diamond paste (up to 1 μm). To prevent crushing of the specimens, thin slices of 2D SiC–SiC material were used to provide end tabs. The grips, particularly designed for tensile tests on ceramic materials, are characterized by an optimum alignment and the suppression of bending and shear moments, obtained by mean of a triaxial rotation capability around the loading point (Schenck, Darmstadt, Germany).

Uniaxial tensile tests were carried out on a servohydraulic Schenck testing machine (Hydropuls PSB) with a 100 kN load cell. A strain gauge with a gauge length of 20 mm was clamped in the central zone of the large side of the specimens. A Dunegan 3000 acoustic emission set, equipped with a piezoelectric transducer of sensitivity 30 to 50 dB between 25 and 625 kHz, was used to monitor precisely the onset of first damage and to record the cumulative number of acoustic emission signals during tests. The tests were force-controlled at a rate of 400 N min^{-1}.

For damage investigation as a function of the applied stress, a set of specimens was loaded at different stress values, σ_i. Once the predetermined stress value was reached, the specimen was totally unloaded and then loaded again until the reloading loop met the preceding unloading loop. This procedure is aimed to allow the measurement of the longitudinal Young's modulus on the reloading loop (E_r) or on the unloading loop (E_u). The specimen was then unloaded for microscopy observation. The damage was evaluated in terms of the total number of transverse microcracks, N, in the gauge length. Counting of the cracks was performed inside a scanning electron microscope (SEM) (Jeol T330, Tokyo, Japan).

3 Results and Discussion

3.1 Stress–strain curve and qualitative study of damage accumulation

To obtain the mechanical characteristics at room temperature and to identify the damage micromechanisms during uniaxial tensile loading, two specimens were loaded monotonically (Fig. 1) and according to loading/unloading procedures.

In situ observations of the specimens during tests using an optical microscope and after the tests in the SEM allowed the micromechanisms activated upon loading this material to be identified. Thus the stress–strain curve can be divided into five regions, each region being characterized by a specific damage micromechanism. This division is schematic because there must be an overlap between different regions, especially as several micromechanisms are generally acting.

(1) The first region ends at point I (ε_{ea} = 0·13%, σ_{ea} = 154 MPa). No damage is detected. The longitudinal Young's modulus is 120 GPa, identical to that estimated (118 GPa) using the rule of mixtures.

(2) The second region extends between I (when the first acoustic counts are recorded at σ_{ae} and ε_{ae}) and the end of linear elastic behaviour corresponding to ε_l = 0·15% and σ_l = 166 MPa. Sporadic acoustic signals were recorded in this region, attesting the initiation of damage which was not observed either by optical microscopy or scanning electron microscopy.

(3) The third domain corresponds to the 'elbow' of the stress–strain curve (ε_l = 0·15% and ε = 0·3%). The beginning of this region is characterized by the presence of short microcracks (Fig. 2). Upon increasing the applied load, they extend along the span of the calibrated zone when other cracks are formed. Acoustic emission activity is extensive in this region.

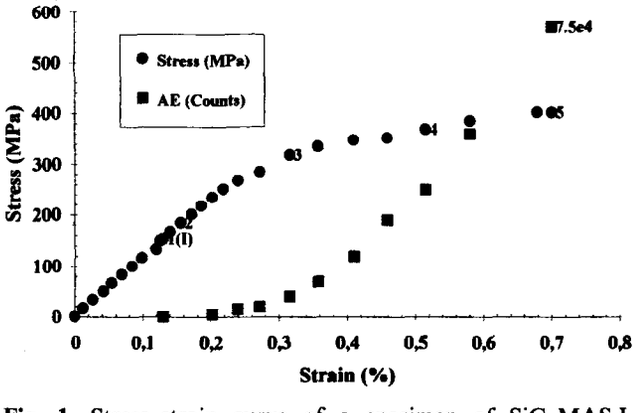

Fig. 1. Stress–strain curve of a specimen of SiC–MAS.L composite material under monotonic loading correlated to acoustic emission records.

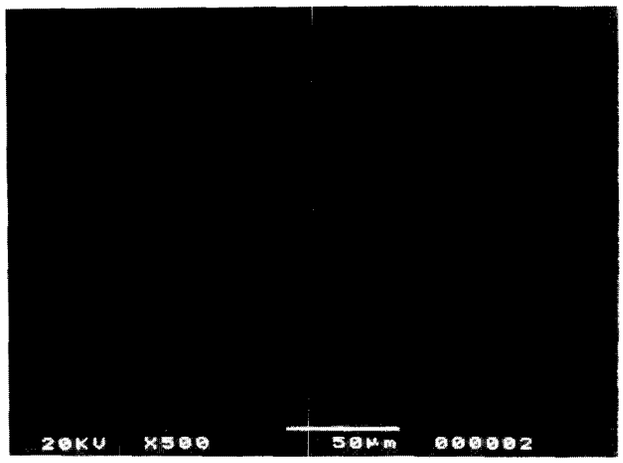

Fig. 2. An example of short transverse matrix microcracks shown on region 3.

Fig. 3. An example of matrix microcrack running parallel to the stress axis.

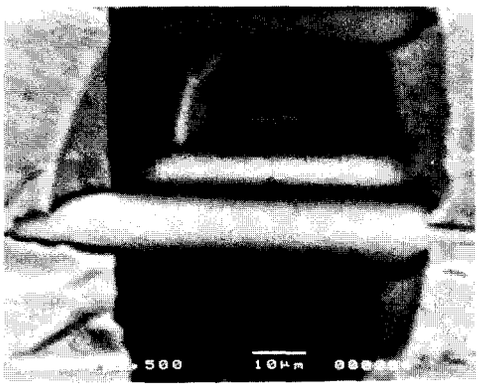

Fig. 4. The opening of transverse microcracks at rupture with bridging fibres.

Fig. 5. The extensive pull-out on the surfaces of rupture.

(4) The fourth region (ε = 0·3 to 0·50%) is characterized by a tangent modulus of 33 GPa. The number of transverse matrix cracks increases. Matrix microcracks running parallel to the stress axis can also be observed (Fig. 3).
(5) In the fifth domain (ε = 0·5% to ε_r), the volume fraction of intact fibres begins to fall with increasing applied stress. In the neighbourhood of the rupture surfaces, the crack openings are very drastic (Fig. 4) and extensive pull-out is revealed (Fig. 5).

3.2 Quantification of transverse matrix microcracking

The method used to quantify the damage accumulation was as follows. The specimens were loaded to different stress levels, σ_i, over the proportional limit. Then the specimen was unloaded and reloaded to measure the longitudinal Young's modulus. When completely unloaded, the damage accumulation was estimated by the total number of transverse matrix cracks created in the calibrated zone length (40 mm). This choice was based on the experimental observations that the number of transverse matrix microcracks N increases in regions 3 and 4 up to a saturation level, N_{sat}, at the beginning of the fifth region.

The transverse matrix microcracks were counted, after total unloading of the specimens, in the SEM at a magnification of > 1000. This experimental procedure is very tedious and time-consuming but has the advantage of being more accurate because of the magnification possibilities of the SEM. Nevertheless, care must be taken. For example, a transverse matrix microcrack must be followed across the entire span of the specimen to prevent multiple counts when crack branching occurs.

Figure 6 presents the total number of transverse matrix microcracks, N, as a function of strain, ε. An important increase of this parameter is noticed up to ε = 0·3%. At a strain of ε = 0·5%, the number of transverse matrix cracks reaches a saturation value close to 250 (N_{sat} = 254). The average crack spacing, $<D>$, deduced from the number of transverse matrix cracks is

$$<D> = L/N \quad (1)$$

where L is the calibrated zone length (40 mm).

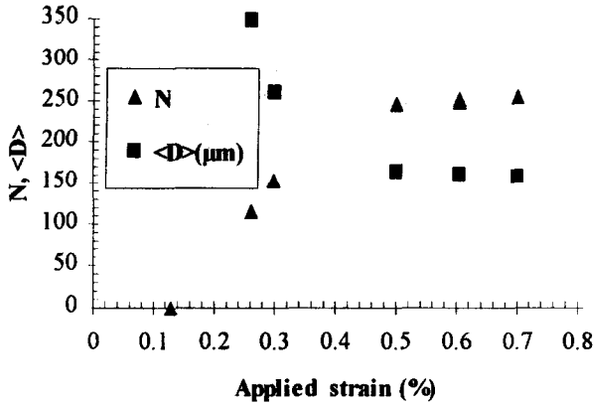

Fig. 6. Evolution of the number of transverse matrix microcracks and the mean crack interspacing as a function of the strain.

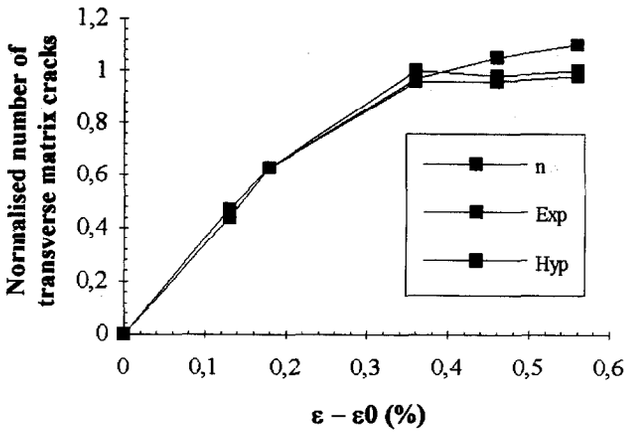

Fig. 7. Change in the $n = N/N_{sat}$ values and those simulated from the exponential (Exp) and hyperbolic (Hyp) functions as a function of the strain.

Using the experimental value of $N_{sat} = 254$, the crack interspacing at saturation is $<D>_{sat} = 160\ \mu m$.

The evolution of the transverse matrix cracks can be described by exponential (i) and hyperbolic (ii) functions.

(i) The exponential law is introduced when writing that the increasing rate of transverse matrix microcracking is proportional to the strain, as previously proposed.[7,8]

$$(dN/dt) \times (dt/d\varepsilon) = k \times (\varepsilon - \varepsilon_0) \quad (2)$$

Then

$$N = N_{sat}\{1-\exp[-\beta \times (\varepsilon - \varepsilon_0)]\} \quad (3)$$

with the parameters $\beta = 6{\cdot}64$ and $\varepsilon_0 = 0{\cdot}15\%$, ε_0 being the proportional strain.

(ii) The hyperbolic function for $\varepsilon > \varepsilon_{ae}$ is given by:

$$n(\varepsilon) = N/N_{sat} = A \times \varepsilon/(\varepsilon + B) \quad (4)$$

with the coefficients $A = 1{\cdot}583$ and $B = 0{\cdot}273$.

Figure 7 shows that both functions provide good fits for experimental results. However, two important points may be noticed.

(1) In the exponential function, the proportional strain ε_0 which is a physical parameter that may be measured experimentally, appears explicitly; this constitutes an important advantage over the hyperbolic function.

(2) Both descriptions are still phenomenological and do not have any theoretical basis. By expressing β as a function of the flaw distribution in the matrix and the corresponding cracking stress levels, it is possible to make the exponential function more significant. Marshall *et al.*[2] have given explanations of that problem for large flaw sizes. However, in the case of small flaw sizes, the solutions proposed by Curtin[4] are still not directly exploitable.

3.3 Evolution of longitudinal Young's modulus

When SiC–MAS.L specimens are loaded cyclically, it is easy to delimit accurately a linear region on the unloading part of the hysteresis loop, but this is not the case on the reloading part.[8] Consequently, the determination of the reloading modulus becomes ambiguous. So, we have taken into account only the unloading modulus, E_u, and the secant modulus, E_s (Fig. 8). On one hand, the evolution of the longitudinal Young's modulus, plotted as a function of strain, shows that E_u decreases more rapidly than E_s from the strain value $\varepsilon = 0{\cdot}2\%$. This behaviour is correlated to the strong increase of the residual deformation from this strain value (Fig. 9). It could be linked to the beginning of opening of matrix microcracks accompanied by fibre failure and contact sliding of the fibres with the matrix. On the other hand, the evolution of the secant modulus could be described correctly by an exponential function as:

$$E_s = E_C \exp[-\alpha \times (\varepsilon - \varepsilon_0)] \quad (5)$$

where E_C is the initial Young's modulus (120 GPa), $\varepsilon_0 = \varepsilon_1 = 0{\cdot}18\%$ with $\alpha = 1{\cdot}54$. As was noticed earlier in the case of the evolution of N, the parameter α can be expressed in terms of the damage micromechanisms acting when testing this composite material.

3.4 Determination of micromechanical parameters

Since the work presented here is interested mainly with the initiation and propagation of the matrix microcracking mechanism with the SiC–MAS.L composite, it is necessary to evaluate the magnitude of the micromechanical parameters influencing this damage micromechanism: i.e. (i) the interfacial shear stress (ISS), which governs the stress transfer at the fibre–matrix interface; (ii) the sign and magnitude of the residual stress, which influence the onset of matrix cracking and the frictional slid-

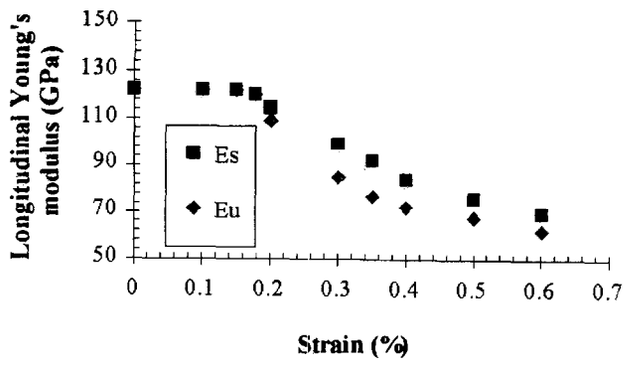

Fig. 8. Evolution of the longitudinal Young's modulus as a function of the strain.

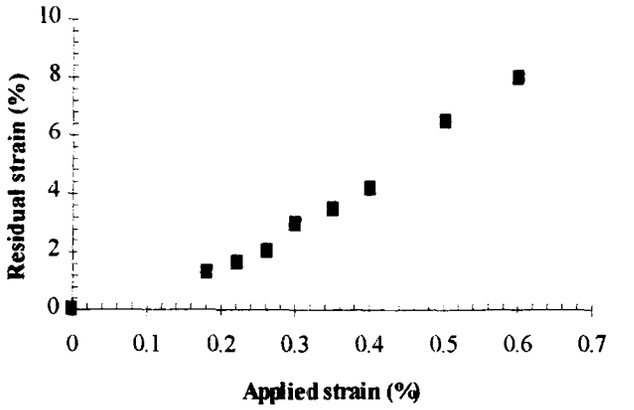

Fig. 9. Evolution of the residual strain as a function of the total applied strain.

ing over debonded regions; (iii) the fracture toughness of the MAS.L matrix; and (iv) the size of the matrix flaws.

3.4.1 Residual stress

The physical characteristics of the matrix and the fibres have been used to estimate the residual stress in the matrix along the fibres, q, and radially in the fibre–matrix interface, p, following the approach of Budiansky *et al.*[9] The residual stresses q and p are given by:

$$q = (\lambda_2/\lambda_1)(E_m E_f V_f \Omega)/E_C(1-\nu) \quad (6)$$

$$p = -E_f(1 - V_f) \times \Omega/[2\lambda_1(1-\nu)] \quad (7)$$

where

$$\lambda_1 = 1-[(1 - 2\nu)/2(1 - \nu)](1 - E_C/E_f) \quad (8)$$

$$\lambda_2 = (1 + E_C/E_f)/2 \quad (9)$$

the thermal strain, Ω, is given by

$$\Omega = (\alpha_m - \alpha_f)(T - T_{amb}) \quad (10)$$

and λ_1 and λ_2 are 0·85 and 0·8, respectively. V_f is the fibre volume fraction and ν is Poisson's ratio. The coefficients of thermal expansion are $\alpha_m = 2{\cdot}1 \times 10^{-6}$ °C^{-1} for the MAS.L matrix[10] and, in the case of the SiC Nicalon fibre, $\alpha_f^L = 3{\cdot}9 \times 10^{-6}$ °C^{-1} and $\alpha_f^T = 2{\cdot}9 \times 10^{-6}$ °C^{-1} in the longitudinal and transverse direction, respectively. The difference between room temperature and the temperature at which the residual stresses can be measured in the composite is 1000°C;[6] the longitudinal Young's modulus of the matrix (E_m) and the fibre (E_f) are 70 GPa and 200 GPa, respectively. Using these values, we obtain the thermal strains $\Omega^L = -0{\cdot}18\%$ and $\Omega^T = -0{\cdot}08\%$ in the longitudinal and transverse directions. Then, the residual stress in the matrix parallel to the fibres is $q = -81$ MPa, and the stress radially in the fibre–matrix interface is $p = 79$ MPa.

Summarizing the results reported above, the fibre–matrix interface is under tension in the radial direction. This special point related to residual stresses is a main parameter that must be properly studied in ceramic matrix composites. Indeed, the sign and magnitude of the residual stresses have an influence on the magnitude of the fibre–matrix friction. This is particularly noticeable in the stress–strain curve along with the evolution of transverse microcracking in the SiC–CAS composite (Figs 10 and 11), where the residual stress p (calculated the same way) is compressive of magnitude $p = -65$ MPa, as shown by Beyerle *et al.*[11] Saturation of the transverse microcracking occurs at a strain value of 0·3%[12] and rigidification of the stress–strain curve from this strain value seems to be strongly influenced by the extensive friction along the fibre–matrix interface.

3.4.2 Interfacial shear stress, τ

The ISS was calculated using the ACK model by ignoring residual stress, as a first approximation. The interfacial shear stress, τ, is given by:[1]

$$\tau = \sigma_{mr} V_m R_f/(2V_f l) \quad (11)$$

where R_f is the fiber radius, V_m is the volume of the matrix $\sigma_{mr} = E_m \sigma_{ae}/E_C = 89$ MPa is the stress of the first matrix cracking, σ_{ae} is the stress corresponding to first acoustic signals ($\sigma_{ae} = 154$ MPa), $E_m = 70$ GPa, $E_f = 200$ GPa, $E_C = 120$ GPa, $l = \langle D \rangle_{sat}/1{\cdot}33$.[13] The calculated value is $\tau = 5{\cdot}5$ MPa. This value is higher than that measured using indentation tests (ranging between 1 and 8 MPa, depending on the radius of the SiC fibres[14]). By comparison, in the case of SiC–LAS composites (which are similar to the SiC–MAS.L material), the ISS is ranged between 1 and 3 MPa. However, in the case of SiC–CAS composites, where the interface is compressive ($p = -65$ MPa), the reported values range between 10 and 20 MPa.[11,12,15]

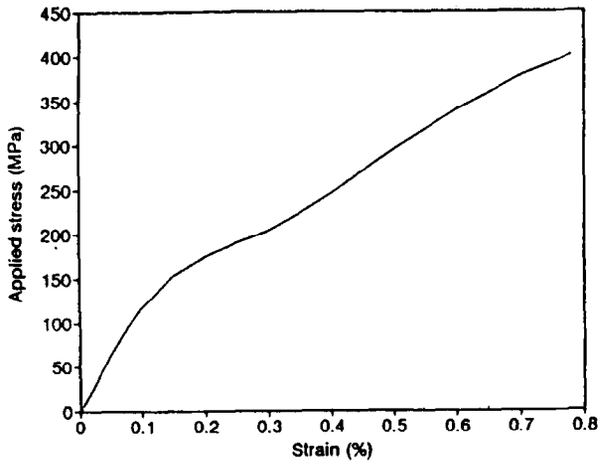

Fig. 10. Representation of the stress–strain curve of an unidirectional SiC–CAS composite, Ref. 12.

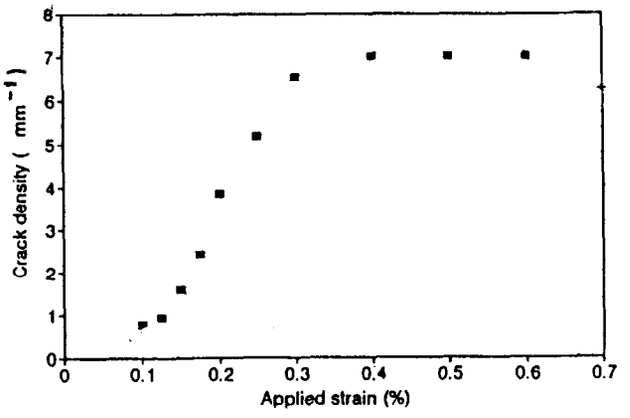

Fig. 11. Evolution of the number of transverse matrix microcracks as a function of the strain in the same composite, Ref. 12.

3.4.3 Estimate of matrix fracture toughness

For reliable measurements of the fracture energy release rate of the MAS.L glass-ceramic matrix, experiments should be done on densified specimens of the matrix along. Owing to a lack of mechanical tests performed directly on the monolithic sol–gel MAS.L glass-ceramic matrix, it is possible to estimate the matrix fracture energy release rate using two procedures.

(i) Suppose that the fracture toughness, K_{IC}^{m}, of the sol–gel matrix is equal to that of the crystallized SiC–MAS.L matrix (1·43 MPa $m^{1/2}$, Ref. 16). In this case and using the Irwin relation

$$\Gamma_m = (K_{IC}^{m})^2/E_m(1 - \nu^2) \quad (12)$$

the as-calculated fracture energy release rate of the MAS.L matrix is $\Gamma_m = 28$ J m^{-2}.

(ii) The second possibility is to use the calculated value of the interfacial shear stress in conjunction with the ACK model. The first microcracking strain in the matrix, ε_{mr}, is given by:[1]

Table 2. Comparison of values of micromechanical parameters obtained in this work for SiC–MAS.L composite with those reported in the literature for similar composite systems

	τ (*MPa*)	Γ_m(*J m* $^{-2}$)	q (*MPa*)
SiC–MAS.L	5·5 MPa	28	–81
SiC–LAS	1–3 (Cao *et al.*[17])	80 (Kim & Pagano,[18])	–50 (Cao *et al.*[17])
SiC–CAS	10–20 (Beyerle *et al.*[11])	25 (Beyerle *et al.*[11])	89 (Beyerle *et al.*[11])

$$\varepsilon_{mr} = (6\tau\Gamma_m E_f V_f^2/E_C E_m^2 R_f V_m)^{1/3} \quad (13)$$

If the residual stress is neglected, the first microcracking strain of the matrix corresponds to $\varepsilon_{ae} = 0{\cdot}13\%$. Then Γ_m is equal to 8 J m^{-2}.

Both values (8 and 28 J m^{-2}) are reasonable for a glass-ceramic matrix and agree well with those reported in the literature for similar materials (ranging between 5 and 80 J m^{-2}, Table 2).

3.4.4 Critical flaw size estimate

Using τ and Γ_m values, we tried to estimate the critical flaw size, a^*, defined from the model of Marshall *et al.*[2] In fact, in the ACK model, the matrix microcracking initiates and continues up saturation at the same stress level. Nevertheless, it is experimentally demonstrated that microcracking initiates and develops over a range of stresses. Marshall *et al.*[2] have correlated this to the existence of two populations of flaws, small and large size flaws delimited by a critical value a^*, given by:

$$a^* = 1/6 \times \Gamma_m^{1/3} \times [V_m R_f E_m^{1/2} E_C/(V_f^2 \tau E_f)]^{2/3} \quad (14)$$

In the case of the SiC–MAS.L composite, $a^* = 43$ μm ($\Gamma_m = 8$ J m^{-2}) and 66 μm ($\Gamma_m = 28$ J m^{-2}). Comparison of these values with the microscopic observations (Fig. 12) shows the existence of a number of flaws with sizes lower than the calculated ones. This point justifies further studies on the spatial distribution of flaws in terms of their

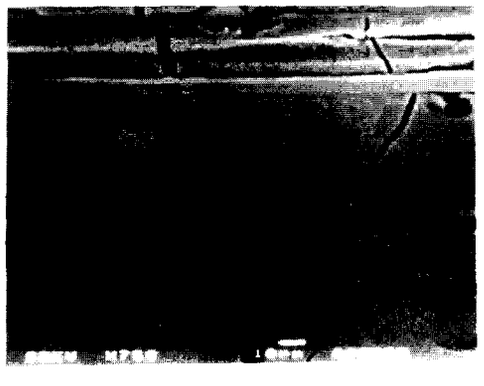

Fig. 12. Micrography representing an example of a MAS.L matrix flaw.

shape and size, because of their strong influence on the mechanical behaviour.

4 Conclusion

In this paper, the damage development in a unidirectional SiC–MAS.L glass-ceramic composite has been evaluated from the number of transverse matrix microcracks, N. This damage parameter, in conjunction with the ACK model, leads to an interfacial shear stress of 5·5 MPa and a matrix fracture energy release rate of 28 J m^{-2}. These values agree with those measured using micromechanical tests. Microscopic observations of the flaw sizes show the existence of sizes lower than the critical one calculated using the model of Marshall *et al.*, justifying a future investigation on the spatial distribution of the matrix flaws in this composite in terms of their size and shape.

Acknowledgements

This work was performed within the French joint programme Groupement Scientifique GS4C (Comportement Thermomécanique des Composites Céramiques à fibres) supported by CNES, CNRS, DRET, MRE and Aérospatiale, SEP and SNECMA companies. We thank Aérospatiale for supplying the specimens.

References

1. Aveston, J., Cooper, G. A. & Kelly, A., Single and multiple fracture in the properties of fiber-composites. In *Proceedings of the National Physical Laboratory*, IPC Science and Technology Press Ltd, London, UK, 1971, pp. 15–26.
2. Marshall, D. B., Cox, B. N. & Evans, A. G., The mechanics of matrix cracking in brittle matrix fiber composites. *J. Am. Ceram. Soc.*, **68**[5] (1985) 225–231.
3. Zok, F. W. & Spearing, S. M., Matrix crack spacing in brittle matrix composites. *Acta Metall. Mater.*, **40**[8] (1992) 2033–2043.
4. Curtin, W. A., Multiple matrix cracking in brittle matrix composites. *Acta Metall. Mater.*, **41**[5] (1993) 1369–1377.
5. Prewo, K. M., Tension and flexural strength of silicon carbide fibre-reinforced glass-ceramics. *J. Mater. Sci.*, **21** (1986) 3590–3600.
6. Larnac, G., Pérès, P. & Donzac, J. M., Elaboration et caractérisation due composite à matrice vitrocéramique SiC–MAS.L. *Rev. Hermès* **3** (1993) 27.
7. Despierres, T., Drissi-Habti, M. & Gomina, M., Damage characterization of a 2D SiC–SiC composite material. *J. Eur. Ceram. Soc.*, **12** (1993) 309–314.
8. Drissi-Habti, M., Despierres, T., Foubert, J. & Gomina, M., Damage investigation on an unidirectional SiC–MAS.L composite under a quasi-static tensile loading. *J. Eur. Ceram. Soc.*, **14** (1994) 91–96.
9. Budiansky, B., Hutchinson J. W. & Evans, A. G., Fracture in fiber-reinforced ceramics. *J. Mech. Phys. Solids*, **34** (1986) 167–189.
10. Villeneuve, PhD Thesis, INSA Lyon, 1991.
11. Beyerle, D. S., Spearing, S. M., Zok, F. W. & Evans, A. G., Damage and failure in unidirectional ceramic-matrix composite. *J. Am. Ceram. Soc.*, **75**[10] (1992) 2719–2725.
12. Pryce, A. W. & Smith, P. A., Behaviour of unidirec-tional and cross-ply ceramic matrix composites under quasi-static tensile loading. *J. Mater. Sci.*, **27** (1992) 2695–2704.
13. Kimber, A. C. & Keer, J. G., On the theoretical average crack spacing in brittle-matrix composites containing aligned fibres. *J. Mater. Sci. Lett.*, **1** (1982) 353.
14. Benoit, M., Brenet, P. & Rouby, D., Comportement des interfaces dans des composites céramique–céramique. *Rev. Compos. Mater. Avancés*, **3** (1993) 235–251.
15. Evans, A. G., AGARO Conference, Antalya, Turkey, 1993. pp. 5-1–5-8.
16. Larnac, G., PhD Thesis, Montpellier, 1989.
17. Cao, H. C., Bishoff, E., Sbaizero, O., Rühle, M., Evans, A. G. & Marshall, D. B., Effects of interfaces on the properties of fiber-reinforced ceramics. *J. Am. Ceram. Soc.*, **73**[6] (1990) 1691–1699.
18. Kim, R. Y. & Pagano, N. J., Crack initiation in unidirectional brittle matrix composites. *J. Am. Ceram. Soc.*, **74**[5] (1991) 1082–1090.